様式第１９

学　会　等　発　表　実　績

委託業務題目「重症薬疹における病期ごとのTh1サイトカインの検討」
機関名　国立大学法人大阪大学

１．学会等における口頭・ポスター発表

発表した成果（発表題目、口頭・ポスター発表の別）	発表者氏名	発表した場所（学会等名）	発表した時期	国内・外の別
Analysis of B cell subsets in severe cutaneous adverse reaction.	Hiroaki Azukizawa, Kenichi Kato, Ichiro Katayama:	The 6th Drug Hypersensitivity Meeting Bern Switzerland	2014.4	国外
手掌に繰り返す紅斑と水疱を引き起こしたアセトアミノフェンによる 固定薬疹.	清原 英司, 小豆澤 宏明, 片山 一朗:	日本皮膚アレルギー・接触皮膚炎学会総会 仙台	2014.11	国内
スピール膏貼付にて蕁麻疹が誘発されたアスピリン不耐症の1例.	藤盛 裕梨, 吉岡 華子, 小豆澤 宏明, 片山 一朗:	日本皮膚アレルギー・接触皮膚炎学会総会 仙台	2014.11	国内
急性汎発性発疹性膿疱症(AGEP)様の皮疹を呈した薬剤過敏症候群(DIHS)の1例.	出口 彩香, 田中 文, 山岡 俊文, 小豆澤 宏明, 片山 一朗, 杉尾 勇太:	日本皮膚アレルギー・接触皮膚炎学会総会 仙台	2014.11	国内
ベバシズマブが誘因と考えられたPerforating dermatosisの1例.	山賀 康右, 花房 崇明, 小豆澤 宏明, 片山 一朗, 小林 真紀, 橋本 直哉:	日本皮膚アレルギー・接触皮膚炎学会総会 仙台	2014.11	国内

２．学会誌・雑誌等における論文掲載

掲載した論文（発表題目）	発表者氏名	発表した場所（学会誌・雑誌等名）	発表した時期	国内・外の別
【重症薬疹の診断と治療】パクリタキセル投与中にみられた顔面紅斑の2例 — Fixed erythrodysaesthesia plaque —	小豆澤　宏明, 横見 明典, 谷 守, 室田 浩之, 中山 貴寛, 玉木 康博, 野口 眞三郎, 片山 一朗:	Journal of Environmental Dermatology and Cutaneous Allergology 8巻2号:109-113	2014.4	国内
Development of Necrotising Fasciitis in a Patient Treated for Rheumatoid Arthritis with Tocilizumab.	Hashimoto N, Yamaoka T, Koguchi-Yoshioka H, Tanaka A, Tanemura A, Azukizawa H, Murota H, Kang J, Nakagawa Y, Shimazu T, Katayama I:	Acta Derm Venereol 95:370-71	2014.8	国外
【重症薬疹の診断と治療アップデート】 重症薬疹の検査.	小豆澤　宏明	アレルギー・免疫 1巻8号:1240-1246	2014.8	国内

Genetic variants associated with phenytoin-related severecutaneous adverse reactions.	Chung WH, Chang WC, Lee YS, Wu YY, Yang CH, Ho HC, Chen MJ, Lin JY, Hui RC, Ho JC, Wu WM, Chen TJ, Wu T, Wu YR, Hsih MS, Tu PH, Chang CN, Hsu CN, Wu TL, Choon SE, Hsu CK, Chen DY, Liu CS, Lin CY, Kaniwa N, Saito Y, Takahashi Y, Nakamura R, Azukizawa H, Shi Y, Wang TH, Chuang SS, Tsai SF, Chang CJ, Chang YS, Hung SI: Taiwan Severe Cutaneous Adverse Reaction Consortium; Japan Pharmacogenomics Data Science Consortium.	JAMA 312:525-34	2014.8	国外
【薬物アレルギー -疑うべきポイントと対処法】薬物アレルギーの発症機序.	小豆澤　宏明	薬事 2014 56巻14号:2135-2140	2014.12	国内
Sequelae in 145 patients with drug-induced hypersensitivity syndrome/drug reaction with eosinophilia and systemic symptoms: Survey conducted by the Asian Research Committee on Severe Cutaneous Adverse Reactions (ASCAR).	Kano Y, Tohyama M, Aihara M, Matsukura S, Watanabe H, Sueki H, Iijima M, Morita E, Niihara H, Asada H, Kabashima K, Azukizawa H, Hashizume H, Nagao K, Takahashi H, Abe R, Sotozono C, Kurosawa M, Aoyama Y, Chu CY, Chung WH, Shiohara T:	J Dermatol (in press)	2015.1	国外

様式第１９

学　会　等　発　表　実　績

委託業務題目「重症薬疹における病因的T細胞の解析」
機関名　学校法人慶応義塾大学

学会等における口頭・ポスター発表

発表した成果（発表題目、口頭・ポスター発表の別）	発表者氏名	発表した場所（学会等名）	発表した時期	国内・外の別
Comparison of basophil activation test and lymphocyte transformation test as diagnostic assays for drug hypersensitivity.	Adachi T, Takahashi H, Funakoshi T, Hirai H, Hashiguchi A, Amagai M, Nagao K:	Drug Hypersensitivity Meeting 6 Bern Switzerland	2014.4	国外
天谷雅行：ゾニサミド内服早期に発症した薬剤性過敏症症候群の1例.	八代聖, 本田皓, 足立剛也, 舩越建, 高橋勇人:	第856回日本皮膚科学会東京地方会 東京	2014.9	国内
薬剤性過敏症症候群長期フォローアップにおける免疫動態の解析-薬剤リンパ球刺激試験と末梢血CD4/8比の有用性-	足立剛也, 高橋勇人, 橋口明彦, 平井博之, 永尾圭介:	第44回日本皮膚アレルギー・接触皮膚炎学会総会学術大会 仙台	2014.11	国内

様式第１９

学　会　等　発　表　実　績

委託業務題目「重症薬疹治療薬の実用化において留意すべき事項」
機関名　国立大学法人北海道大学

１．学会等における口頭・ポスター発表

発表した成果（発表題目、口頭・ポスター発表の別）	発表者氏名	発表した場所（学会等名）	発表した時期	国内・外の別
日本で承認された患者数が特に少ない希少疾病用医薬品の臨床データパッケージについて.	荒戸照世, 金子真之, 前田浩次郎, 成川衛:	第4回レギュラトリーサイエンス学会学術集会 東京	2014.9	国内
患者数が特に少ない希少疾病用医薬品の臨床評価のポイントについて.	前田浩次郎, 金子真之, 成川衛, 荒戸照世:	第35回日本臨床薬理学会学術総会 松山	2014.12	国内
実用化研究はレギュラトリーサイエンスの実践教育.	荒戸照世	日本薬学会135年会 神戸	2015.3	国内

２．学会誌・雑誌等における論文掲載

掲載した論文（発表題目）	発表者氏名	発表した場所（学会誌・雑誌等名）	発表した時期	国内・外の別
アカデミアにおけるトランスレーショナル・リサーチの現状と課題.	荒戸照世, 佐藤典宏:	バイオサイエンスとインダストリー Vol.72 No.4:334-338	2014.7	国内

Ⅳ. 研究成果の刊行物・別刷

CUTANEOUS DRUG REACTIONS

An annexin A1–FPR1 interaction contributes to necroptosis of keratinocytes in severe cutaneous adverse drug reactions

Nao Saito,[1] Hongjiang Qiao,[1] Teruki Yanagi,[1] Satoru Shinkuma,[1] Keiko Nishimura,[1] Asuka Suto,[1] Yasuyuki Fujita,[1] Shotaro Suzuki,[1] Toshifumi Nomura,[1] Hideki Nakamura,[1] Koji Nagao,[2] Chikashi Obuse,[2] Hiroshi Shimizu,[1]* Riichiro Abe[1]*

Stevens-Johnson syndrome (SJS) and toxic epidermal necrolysis (TEN) are life-threatening, cutaneous adverse drug reactions that are accompanied by keratinocyte cell death. Dead keratinocytes from SJS/TEN lesions exhibited necrosis, by morphological criteria. Supernatant from peripheral blood mononuclear cells (PBMCs) that had been exposed to the causative drug from patients with SJS/TEN induced the death of SJS/TEN keratinocytes, whereas supernatant from PBMCs of patients with ordinary drug skin reactions (ODSRs) exposed to the same drug did not. Keratinocytes from ODSR patients or from healthy controls were unaffected by supernatant from SJS/TEN or ODSR PBMCs. Mass spectrometric analysis identified annexin A1 as a key mediator of keratinocyte death; depletion of annexin A1 by a specific antibody diminished supernatant cytotoxicity. The necroptosis-mediating complex of RIP1 and RIP3 was indispensable for SJS/TEN supernatant–induced keratinocyte death, and SJS/TEN keratinocytes expressed abundant formyl peptide receptor 1 (FPR1), the receptor for annexin A1, whereas control keratinocytes did not. Inhibition of necroptosis completely prevented SJS/TEN-like responses in a mouse model of SJS/TEN. Our results demonstrate that a necroptosis pathway, likely mediated by annexin 1 acting through the FPR1 receptor, contributes to SJS/TEN.

INTRODUCTION

Stevens-Johnson syndrome (SJS) and toxic epidermal necrolysis (TEN) are rare, life-threatening adverse drug reactions characterized by extensive detachment of the epidermis. They are considered as part of the same spectrum of diseases, but SJS patients have skin detachment on less than 10% of the body surface area, whereas TEN patients have more extensive lesions (*1*). After causative drug intake, the eruptions show erythema, and then the skin lesions spread to the whole body and become erosions. Mucous membranes are involved in about 90% of patients. Although SJS and TEN are rare (seven cases and two cases per million population for SJS and TEN, respectively), the mortality rates are high: up to 5 and 30% for SJS and TEN (*1*). The cause is thought to be the induction of an immunological reaction by the causative drugs. In patients with SJS/TEN, $CD8^+$ T cells are the predominant cell population that infiltrates the epidermis of the lesions (*2*), and drug-specific $CD8^+$ T cells proliferate predominantly in peripheral blood (*3*). Keratinocyte death in SJS/TEN has been thought to result from the action of cytotoxic cells or soluble factors such as soluble FasL or granulysin (*2*, *4*, *5*). Keratinocytes have been suggested to die by apoptosis (*4*), although the precise mechanism of keratinocyte death in SJS/TEN remains unclear.

Cell death generally has been thought to be initiated by a regulated signaling pathway, known as apoptosis, or by an unregulated process resulting from cellular damage, known as necrosis. This paradigm has been challenged by findings that necrosis can also result from programmed signaling (*6*). Under some conditions, stimulation with Fas ligand or tumor necrosis factor–α (TNF-α) can induce cell death that has the morphological features of necrosis (*7*, *8*). Recently, the RIP1/RIP3 complex was found to play a major role in necroptosis, and multiple small-molecule inhibitors of necroptosis, or "necrostatins," were discovered (*9*, *10*). Necroptosis is now recognized as a cellular defense mechanism against viral infections and as being critically involved in ischemia-reperfusion damage (*9*). Paneth cells in Crohn's disease have been reported to show programmed necrosis (*11*, *12*).

Here, we investigate how keratinocytes die in SJS/TEN. Drug-specific lymphocytes exist in patients who have recovered from drug allergies, including SJS/TEN (*13*–*15*). We searched for cytotoxic agents that might be secreted from these drug-specific lymphocytes by examining the supernatant of causative drug–exposed peripheral blood mononuclear cells (PBMCs) from recovered SJS/TEN patients.

RESULTS

SJS/TEN keratinocyte death by necroptosis

To investigate the nature of keratinocyte death in SJS/TEN, we examined the morphological changes in active lesions of SJS/TEN that showed marked epidermal cell death by electron microscopy (Fig. 1, A to C). To ensure that keratinocyte death was not necrosis resulting from ischemic or mechanical stress, we obtained all samples from erythematous lesions of SJS/TEN that showed nonbullous skin eruptions clinically and no epidermis-dermis detachment histologically. We found that some keratinocytes showed necrotic morphology, including membrane breakdown and numerous swollen cellular organelles (Fig. 1B). Other keratinocytes showed a reduction of cellular volume and chromatin condensation, features compatible with apoptotic morphology (Fig. 1C). Necrotic and apoptotic cells represented 16.1 ± 2.1% and 10.5 ± 0.7%, respectively, of all keratinocytes ($N = 80$) in the SJS/TEN lesions. Therefore, morphological apoptosis and necrosis both occur in erythematous lesions of SJS/TEN.

We next hypothesized that, upon initial drug stimulation, drug-specific lymphocytes secrete a soluble factor that induces widespread cutaneous

[1]Department of Dermatology, Hokkaido University Graduate School of Medicine, Sapporo 060-8638, Japan. [2]Graduate School of Life Science, Hokkaido University, Sapporo 060-0810, Japan. *Corresponding author. E-mail: aberi@med.hokudai.ac.jp (R.A.); shimizu@med.hokudai.ac.jp (H.S.)

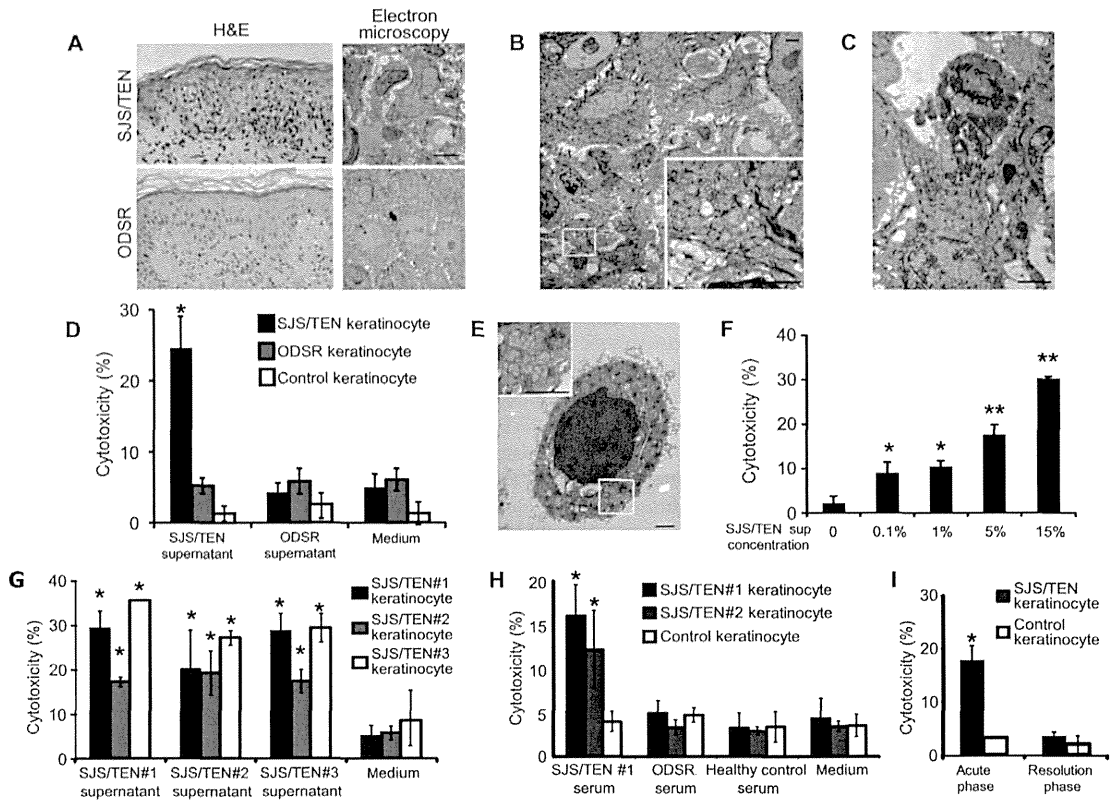

Fig. 1. Keratinocyte death in SJS/TEN shows necrotic and apoptotic morphology. (**A**) Morphological keratinocyte changes in SJS/TEN lesions and ODSRs were observed by hematoxylin and eosin (H&E) staining and electron microscopy, representative image. Scale bars, 10 μm (H&E) and 3 μm (electron microscopy). Skin samples were obtained from patient nos. 10 (early lesion) and 18 (early lesion). (**B** and **C**) Representative images of necrotic (B) and apoptotic (C) keratinocyte changes seen in SJS/TEN lesions by electron microscopy. (Inset) Swollen mitochondria. Scale bar, 5 μm. (**D**) Keratinocytes from SJS/TEN patients, ODSR patients, or healthy controls were exposed to supernatants from causative drug–exposed PBMCs for 8 hours. Cytotoxicity was measured by trypan blue staining ($n = 4$). *$P < 0.01$. Keratinocytes and PBMCs were obtained from patient no. 3 (postlesional skin), patient no. 14 (postlesional skin), and healthy control no. 6. (**E**) Representative image of SJS/TEN supernatant–exposed SJS/TEN keratinocytes showing necrotic morphology including swollen mitochondria (insert) by electron microscopy. Scale bar, 5 μm. Keratinocytes were obtained from patient no. 3 (postlesional skin). (**F**) Dose dependence of cytotoxicity by SJS/TEN supernatant (sup) was analyzed ($n = 4$). *$P < 0.05$; **$P < 0.01$. Keratinocytes and PBMCs were obtained from patient no. 5 (nonlesional skin). (**G**) Cytotoxicity of SJS/TEN supernatant (5%) on SJS/TEN keratinocytes from three patients. Each experiment was repeated five times. *$P < 0.01$ versus medium. Keratinocytes and PBMCs were obtained from patient nos. 3 (postlesional skin), 4 (nonlesional skin), and 8 (nonlesional skin). (**H**) Keratinocytes from SJS/TEN patients or healthy controls were exposed to sera of patients with SJS/TEN or ODSR, and healthy controls for 8 hours. Cytotoxicity was measured by trypan blue staining ($n = 4$). *$P <$ 0.01. Keratinocytes were obtained from patient no. 4 (nonlesional skin), patient no. 10 (postlesional skin), and healthy control no. 9. Sera were obtained from patient no. 4, patient no. 18, and healthy control no. 2. (**I**) Cytotoxicity of SJS/TEN serum during disease onset (acute phase) and after recovery (resolution phase) ($n = 5$). *$P < 0.01$. Keratinocytes were obtained from patient no. 1 (postlesional skin) and healthy control no. 5. Sera were obtained from patient no. 1.

detachment through keratinocyte death. The lymphocytes that specifically reacted with the causative drug then may remain in peripheral blood of recovered SJS/TEN patients, and upon reexposure to the causative drug, these lymphocytes would again secrete the key soluble factor(s). To test for the presence of causative drug–specific lymphocytes in peripheral blood in recovered patients, we collected PBMCs from patients ($n = 6$) who had recovered from SJS/TEN 1 to 5 years before. Enzyme-linked immunospot (ELISPOT) analysis of human interferon-γ (IFN-γ) secretion was conducted to detect antigen-specific human cells; we detected causative drug–specific lymphocytes (fig. S1). After in vitro reexposure to the causative drug, the number of drug-specific lymphocytes increased markedly (fig. S1). These data confirmed that, even after the resolution of SJS/TEN, drug-specific lymphocytes still circulate, as reported (*13*, *14*).

To test for toxic agents that might be secreted by drug-specific lymphocytes, we exposed PBMCs from recovered SJS/TEN patients to the causative drugs and then collected the supernatants. Treatment of keratinocytes from SJS/TEN patients with SJS/TEN supernatant resulted in cell death, whereas treatment of SJS/TEN keratinocytes with supernatant from PBMCs from patients with ordinary drug skin reactions (ODSRs) and other types of severe adverse drug reactions [drug-induced hypersensitivity syndrome (DIHS)/drug reaction with eosinophilia and systemic symptoms (DRESS)] had no effect on keratinocytes (Fig. 1D and fig. S2). Keratinocytes from

ODSR patients or healthy controls were unaffected by SJS/TEN and ODSR supernatant.

We examined the morphological changes in supernatant-treated keratinocytes by electron microscopy. The supernatant-exposed keratinocytes showed swollen mitochondria and blebbing of the cellular membrane, reactions compatible with necrotic morphology (Fig. 1E). Necrotic and apoptotic cells accounted for 76.7 ± 5.8% and 23.3 ± 5.8% of dead keratinocytes (n = 35), respectively.

SJS/TEN supernatant induced cytotoxicity against SJS/TEN keratinocytes in a dose-dependent manner (Fig. 1F). SJS/TEN supernatant from three recovered patients and SJS/TEN keratinocytes from the same patients showed significant cytotoxicity in each combination (Fig. 1G). Furthermore, we analyzed the cytotoxicity of supernatants from PBMCs of a SJS/TEN patient (case 5 in table S2) exposed to an irrelevant drug (amoxicillin). The supernatants from PBMCs exposed to the irrelevant drug did not induce cytotoxicity (fig. S3).

Because the previous experiments used samples from patients who had recovered from SJS/TEN, we tested whether a cytotoxic soluble factor was also present in peripheral blood during the active phase of SJS/TEN. Sera from patients with active SJS/TEN were incubated with SJS/TEN keratinocytes and found to cause cytotoxicity, whereas sera from patients with ODSR did not (Fig. 1H). The keratinocytes of ODSR patients or healthy controls were unaffected by SJS/TEN and ODSR sera. In addition, we investigated the direct cytotoxicity of sera from patients who were in the SJS/TEN recovery phase. These sera did not induce cytotoxicity (Fig. 1I).

To determine whether keratinocytes taken from healed postlesional skin and keratinocytes taken from nonlesional skin differed in sensitivity to the putative toxic agent, we compared SJS/TEN PBMC supernatant–induced cytotoxicity in keratinocytes from these two sites (fig. S4A). We obtained the cultured keratinocytes from normal-appearing skin that had been lesional during the acute phase but that had returned to normal (postlesional; n = 3) or from normal-appearing skin that was never lesional (nonlesional; n = 4). SJS/TEN PBMC supernatant induced comparable cytotoxicity in both cases (fig. S4B).

Apoptosis is dependent on the activation of caspases; necroptosis is not influenced by caspase inhibition but is blocked by necrostatin-1 (Nec-1), an inhibitor of the kinase activity of RIP1 and by RIP3 inhibition (*9*). To test whether SJS/TEN supernatant–induced cytotoxicity is apoptosis, we investigated the cleavage of poly(adenosine 5′-diphosphate–ribose) polymerase (PARP), a substrate of cleaved caspase-3. Cleaved PARP was not detected in keratinocytes treated with SJS/TEN supernatant (Fig. 2A).

To further investigate the mechanism of SJS/TEN supernatant–induced cytotoxicity, we examined the effect of the pan-caspase inhibitor zVAD and the necroptosis inhibitor Nec-1 on SJS/TEN supernatant–induced keratinocyte death. Although zVAD did not inhibit cytotoxicity, Nec-1 completely inhibited cytotoxicity (Fig. 2B). In addition, to clarify the role of RIP3 in our cytotoxic process, we knocked down RIP3 with small interfering RNA (siRNA), which significantly decreased the cytotoxicity of the SJS/TEN supernatant (Fig. 2C). In the SJS/TEN lesions, the keratinocytes showed abundant RIP3 expression, just as necroptotic Paneth cells do in Crohn's disease (*12*). In contrast, no cells showed RIP3 expression in ODSR lesions (Fig. 2D). These data suggest that necroptosis can contribute to keratinocyte death in SJS/TEN.

Some cell lines are capable of undergoing necroptosis in response to cytokines of the TNF family (*16*). In this pathway, TNF-α reacts with the TNF-α receptor, forming a complex with FADD (Fas-associated protein with death domain) and RIP1/RIP3, after MLKL phosphorylation (*17*, *18*). To investigate whether these molecules also control keratinocyte-programmed necrosis, we analyzed the expressions of RIP1, RIP3, FADD, and CYLD in keratinocytes. Expression levels of these molecules varied among keratinocytes from SJS/TEN patients, ODSR patients, or healthy controls (fig. S5), indicating that the levels of these molecules were not regulating the susceptibility to keratinocyte necroptosis.

Necroptosis by annexin A1–formyl peptide receptor 1 interaction

To try to identify the necroptosis mediators in the SJS/TEN supernatant, we tested apoptosis inducers such as granulysin and necroptosis agents such as TNF-α, poly(I:C) (polyinosinic-polycytidilic acid), or LPS (lipopolysaccharide), but found that they failed to induce SJS/TEN keratinocyte death (fig. S6). Therefore, we performed mass spectrometry [liquid chromatography–tandem mass spectrometry (LC-MS/MS)] of SJS/TEN and ODSR supernatants and identified the protein annexin A1 as significantly more abundant in SJS/TEN supernatant than in ODSR supernatant (table S1 and Fig. 3A). To test the importance of annexin A1, we depleted it from SJS/TEN supernatant using a specific annexin A1 antibody, which significantly blocked SJS/TEN supernatant–induced keratinocyte death (Fig. 3B). Moreover, the annexin A1–mimetic peptide Ac2-26 induced cytotoxicity in SJS/TEN keratinocytes, but not in healthy control keratinocytes

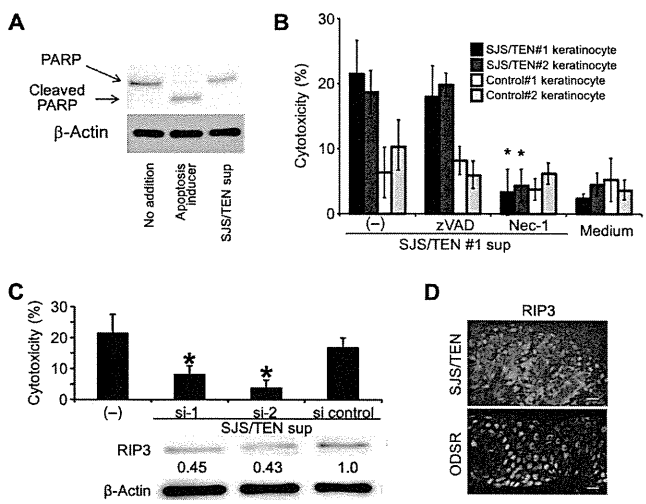

Fig. 2. Keratinocyte death by PBMC supernatant from SJS/TEN patients is mediated by necroptosis. (**A**) PARP cleavage assay was performed with apoptosis inducer (2 μM staurosporine) or SJS/TEN supernatant (5%). Keratinocytes and PBMCs were obtained from patient no. 3 (postlesional skin). The experiments were repeated three times, and representative data are shown. (**B**) Effects of the pan-caspase inhibitor zVAD (50 μM) or Nec-1 (50 μM) on cytotoxicity were analyzed (n = 4). *P < 0.01 versus SJS#1 sup alone. Keratinocytes were obtained from patient no. 3 (postlesional skin), patient no. 4 (nonlesional skin), healthy control no. 8, and healthy control no. 10, and PBMCs from patient no 3. (**C**) RIP3 was knocked down with siRNA (si-1 or si-2) in SJS/TEN keratinocytes, and SJS/TEN supernatant–induced cytotoxicity was analyzed (n = 4). Densitometric values are shown as percent optical density of RIP3 in siRNA-transfected cells after β-actin normalization. *P < 0.05 versus siRNA control. Keratinocytes and PBMCs were obtained from patient no. 3 (postlesional skin). (**D**) Representative image of RIP3 expression in SJS/TEN lesions and ODSRs. Nuclei were stained with propidium iodide (PI). Scale bars, 10 μm. Skin samples were obtained from patient nos. 10 (early lesion) and 18 (early lesion).

(Fig. 3C). Although annexin A1 is an intracellular molecule, it is also secreted from $CD14^+$ monocytes, where it acts as an immunosuppressant (*19*). To test for the source of annexin A1, we depleted $CD14^+$ monocytes from SJS/TEN PBMCs that were exposed to the causative drug, and these PBMCs failed to induce SJS/TEN keratinocyte death (Fig. 3D), confirming $CD14^+$ cells as the likely source of annexin A1. Indeed, $CD14^+$ cells are present in SJS/TEN skin lesions (*20*).

$CD14^+$ monocytes can be divided into at least two populations: $CD14^{bright}$ classical monocytes and $CD14^{dim}$ proinflammatory monocytes. Both cell types induced cytotoxicity (fig. S7). Monocyte activation is not mediated by a specific antigen. However, we and other groups have reported that $CD8^+$ cells and major histocompatibility complex (MHC) class I are indispensable in SJS/TEN pathogenesis (*4*, *15*). Therefore, we suggest that $CD8^+$ cell activation by a specific antigen (the causative drug) or by MHC class I is critical for the secretion of annexin A1 from monocytes. First, supernatant from $CD14^+$-depleted PBMCs failed to induce cytotoxicity (Fig. 3D). Furthermore, supernatant from $CD14^+$ plus CD14-depleted supernatant succeeded in killing keratinocytes (Fig. 3E). Supernatant

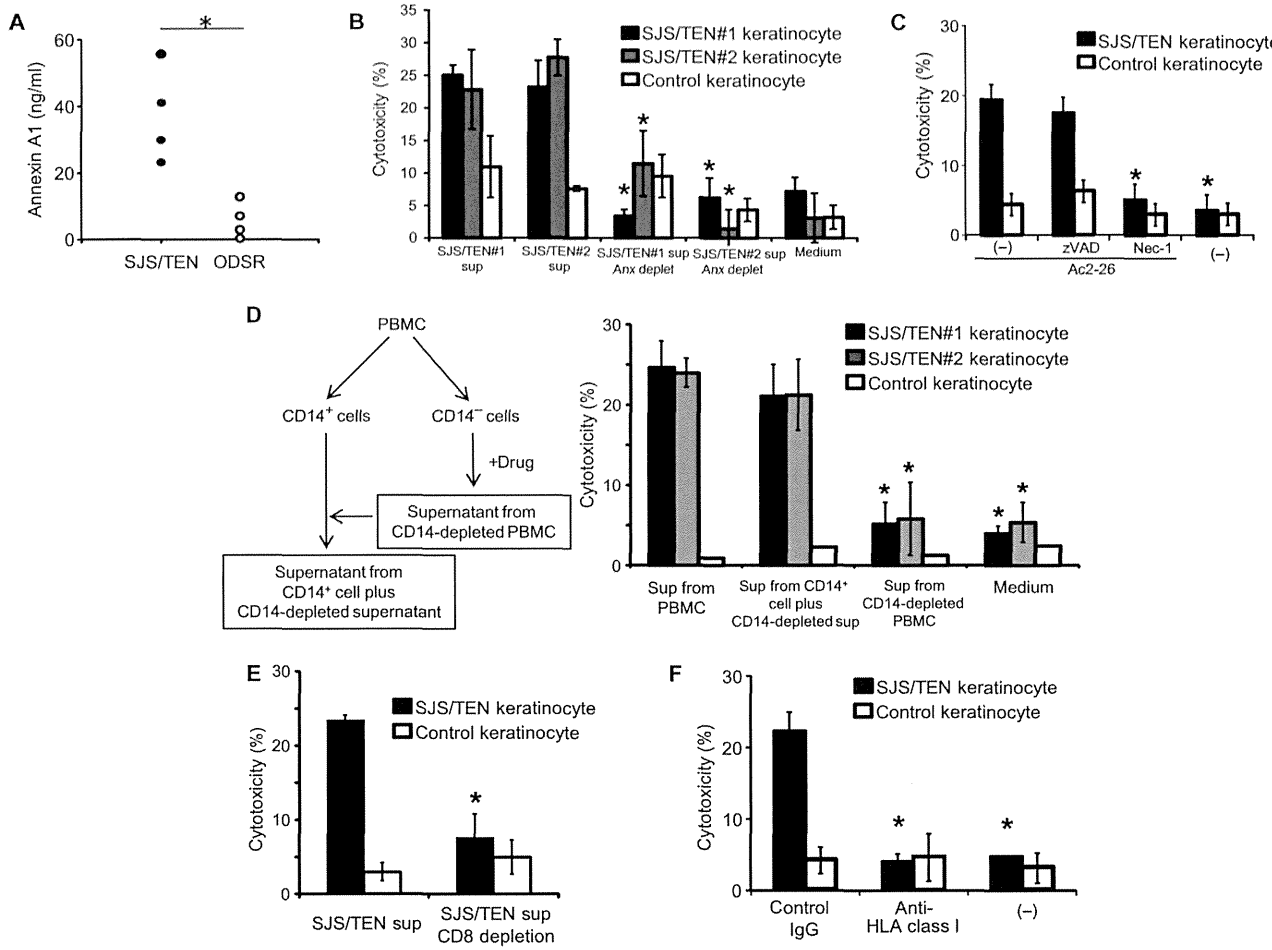

Fig. 3. Annexin A1 mediates necrosis caused by PBMC supernatant from SJS/TEN patients. (**A**) Annexin A1 concentrations were measured by annexin A1 peptide enzyme-linked immunosorbent assay (ELISA) in supernatants collected from causative drug–exposed PBMCs of SJS/TEN ($n = 4$) and ODSR ($n = 4$) patients. *$P < 0.05$. PBMCs were obtained from patient nos. 3, 4, 5, 6, 11, 12, 14, and 17. Each point was measured three times. (**B**) Cytotoxicity assay using annexin A1–depleted SJS/TEN supernatant ($n = 5$). *$P < 0.05$ versus SJS/TEN sup. Keratinocytes and PBMCs were obtained from patient no. 3 (postlesional skin) and no. 5 (nonlesional skin). Keratinocytes were obtained from healthy control no. 4. (**C**) Effect of annexin A1 peptide (Ac2-26) (50 ng/ml) on cytotoxicity in SJS/TEN keratinocytes ($n = 5$). *$P < 0.05$ versus Ac2-26. Keratinocytes were obtained from patient no. 5 (nonlesional skin) and healthy control no. 3. (**D**) Effect of CD14-depleted supernatant and supernatant from $CD14^+$ cells plus CD14-depleted supernatant on cytotoxicity of keratinocytes. ($n = 5$). *$P < 0.01$ versus supernatant from PBMC. Keratinocytes were obtained from patient no. 3 (postlesional skin), patient no. 5 (nonlesional skin), and healthy control no. 7. PBMCs were obtained from patient no. 3. (**E**) Effect of $CD8^+$ cells on SJS/TEN PBMC supernatant–induced cytotoxicity. Supernatant from $CD8^+$ cell–depleted SJS/TEN PBMCs with causative drug exposure was analyzed for cytotoxicity ($n = 5$). *$P < 0.05$ versus SJS/TEN supernatant. Keratinocytes were obtained from patient no. 3 (postlesional skin) and healthy control no. 8. PBMCs were obtained from patient no. 3. (**F**) Effect of anti–MHC class I antibody on SJS/TEN supernatant–induced cytotoxicity. SJS/TEN PBMCs were preincubated for 30 min at 37°C with anti–MHC I antibody (10 μg/ml) or control mouse IgG ($n = 5$). *$P < 0.05$ versus SJS/TEN supernatant. Keratinocytes were obtained from patient no. 10 (postlesional skin) and healthy control no. 5. PBMCs were obtained from patient no. 2.

from $CD8^+$-depleted PBMCs did not induce cytotoxicity (Fig. 3F). In addition, we collected supernatant from causative drug–exposed PBMCs that had been cultured with neutralizing MHC class I antibody (W6/32). The cytotoxicity of the supernatant was greatly decreased; in contrast, the supernatant from causative drug–exposed PBMCs that had been cultured with control mouse immunoglobulin G (IgG) did not show reduced cytotoxicity (Fig. 3G). Together, these data show that $CD8^+$ cell activation by a specific antigen (the causative drug) or by MHC class I is critical to cytotoxicity.

Finally, we investigated the roles of $CD14^+$ and $CD8^+$ cells in SJS/TEN model mice that we have recently developed (*15*) (Fig. 4A). These mice, generated by using SJS/TEN PBMCs and causative drugs (*15*), show eye manifestations of disease (marked conjunctival congestion) (Fig. 4B). If we used $CD14^+$-depleted PBMCs or $CD8^+$-depleted PBMCs during generation of these model mice, the development of the conjunctival congestion was prevented. $CD8^+$-depleted PBMCs also failed to induce SJS/TEN-like symptoms (conjunctival epithelial cell death) in the model mice (Fig. 4C).

Annexin A1 binds to formyl peptide receptor 1 (FPR1) and acts via that receptor (*19*). FPR1 is in the family of G protein (heterotrimeric guanine nucleotide–binding protein)–coupled receptors and is associated with tissue damage (*21*). When treated with SJS/TEN supernatant, SJS/TEN keratinocytes expressed abundant FRP1 in vitro, whereas

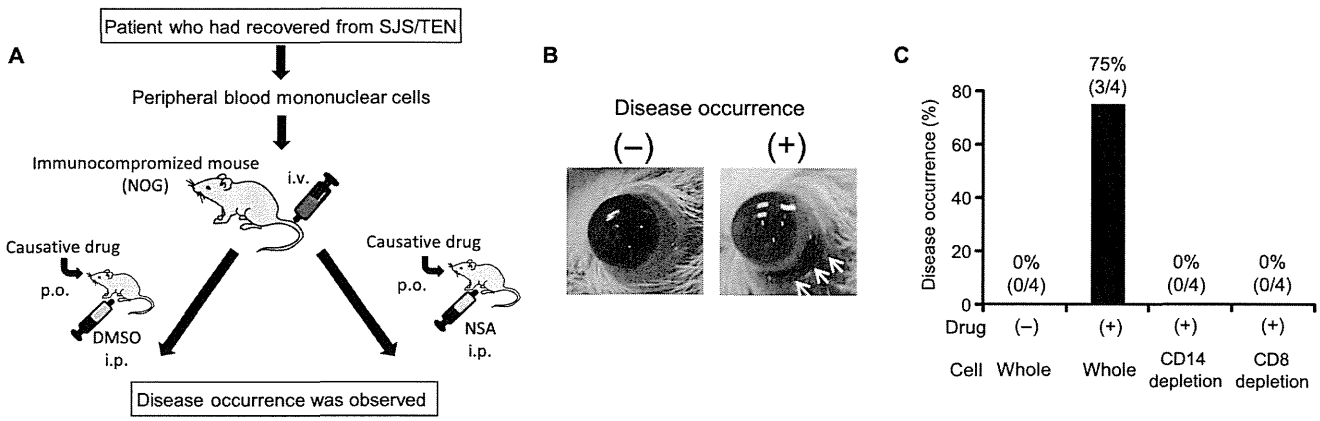

Fig. 4. $CD14^+$ and $CD8^+$ cells are required for pathogenesis in a mouse model of SJS/TEN model mice. (**A**) PBMCs were obtained from patients who had recovered from SJS/TEN. PBMCs, $CD14^+$-depleted PBMCs, or $CD8^+$-depleted PBMCs (2×10^6) were injected intravenously into NOG [nonobese diabetic (NOD)/Shi-scid, interleukin-1 receptor (IL-2R) null] mice, followed by oral administration of the causative drug. The dosage used in the model mice was based on mg/kg body weight converted from human adult normal dose. We administered the drug to the mice once daily. In addition, these mice received necrosulfonamide (NSA) or dimethyl sulfoxide (DMSO) intraperitoneally. The mice were observed for eye manifestations of disease. PBMCs were obtained from patient nos. 2 and 3. (**B**) SJS/TEN model mice were established by intravenous injection of PBMCs obtained from SJS/TEN patients and oral administration of the causative drugs. SJS/TEN model mice showed eye dysfunction (marked conjunctival congestion), as shown in the representative photos. PBMCs were obtained from patient no. 3. (**C**) Effect of CD14 and CD8 depletion on the ability of SJS/TEN PBMCs to cause SJS-like disease in model mice ($n = 4$).

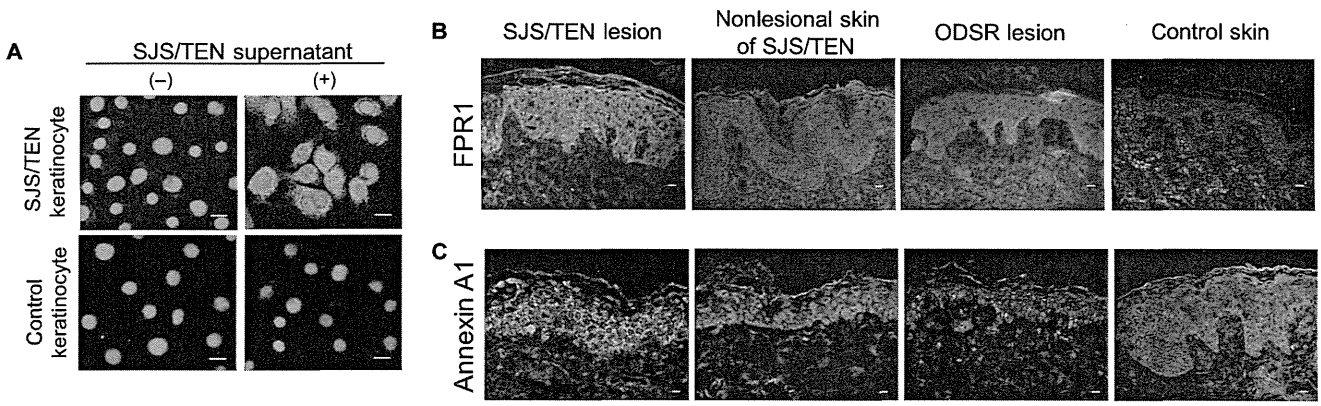

Fig. 5. SJS/TEN keratinocytes express FRP1. (**A**) Representative images of FRP1 in cultured keratinocytes from SJS/TEN patients or healthy controls. Cultured cells were treated with or without SJS/TEN supernatant (5%) (4 hours) and were stained for FRP1 with an antibody ($n = 3$). Representative data are shown. Nuclei were stained with PI. Scale bars, 5 μm. Keratinocytes were obtained from patient no. 3 (postlesional skin) and healthy control no. 4. (**B** and **C**) Representative images showing expression of FRP1 and annexin A1 in SJS/TEN lesions, nonlesional skin of SJS/TEN patients, ODSR lesions, and control skin. Nuclei were stained with PI. Scale bars, 10 μm. Skin samples were obtained from patient no. 10 (acute lesion and nonlesional skin), patient no. 18 (acute lesion), and healthy control no. 4.

control keratinocytes did not (Fig. 5A). In addition, FRP1-positive cells were detected in SJS/TEN lesions, whereas no FRP1-positive cells were detected in the nonlesional skin of SJS/TEN, ODSR lesions, or normal skin (Fig. 5B). Abundant annexin A1 was also detected in the SJS/TEN lesions; in contrast, little annexin A1 was seen in the nonlesional skin of SJS/TEN, in ODSR lesions, or in normal skin (Fig. 5C). When SJS/TEN keratinocytes were exposed to *N*-formyl-Met-Leu-Phe (*f*MLP), which is an FPR1 ligand, they showed a cytotoxic response, whereas no effects were seen in healthy control keratinocytes (Fig. 6A). Moreover, Nec-1 effectively inhibited *f*MLP-induced SJS/TEN keratinocyte death. A neutralizing antibody against FPR1 prevented SJS/TEN supernatant–induced cytotoxicity (Fig. 6B). *f*MLP induced cytotoxicity in SJS/TEN keratinocytes in a dose-dependent manner (Fig. 6C). FPR2 is also a receptor for annexin A1 (*22*), but when we added an FPR2 antagonist (WRW4) (Trp-Arg-Trp-Trp-Trp-Trp) (0.1 or 1.0 μM) during SJS/TEN supernatant–induced cytotoxicity, cytotoxicity was not inhibited (Fig. 6D).

FPR1 has not previously been known to relate to both apoptosis and necroptosis. To show that the FPR1 signal stimulates a necroptosis pathway, we analyzed the RIP1/RIP3 immunocomplex obtained from a Flag-tagged RIP3 pull-down in Flag-RIP3-HeLa cells. We

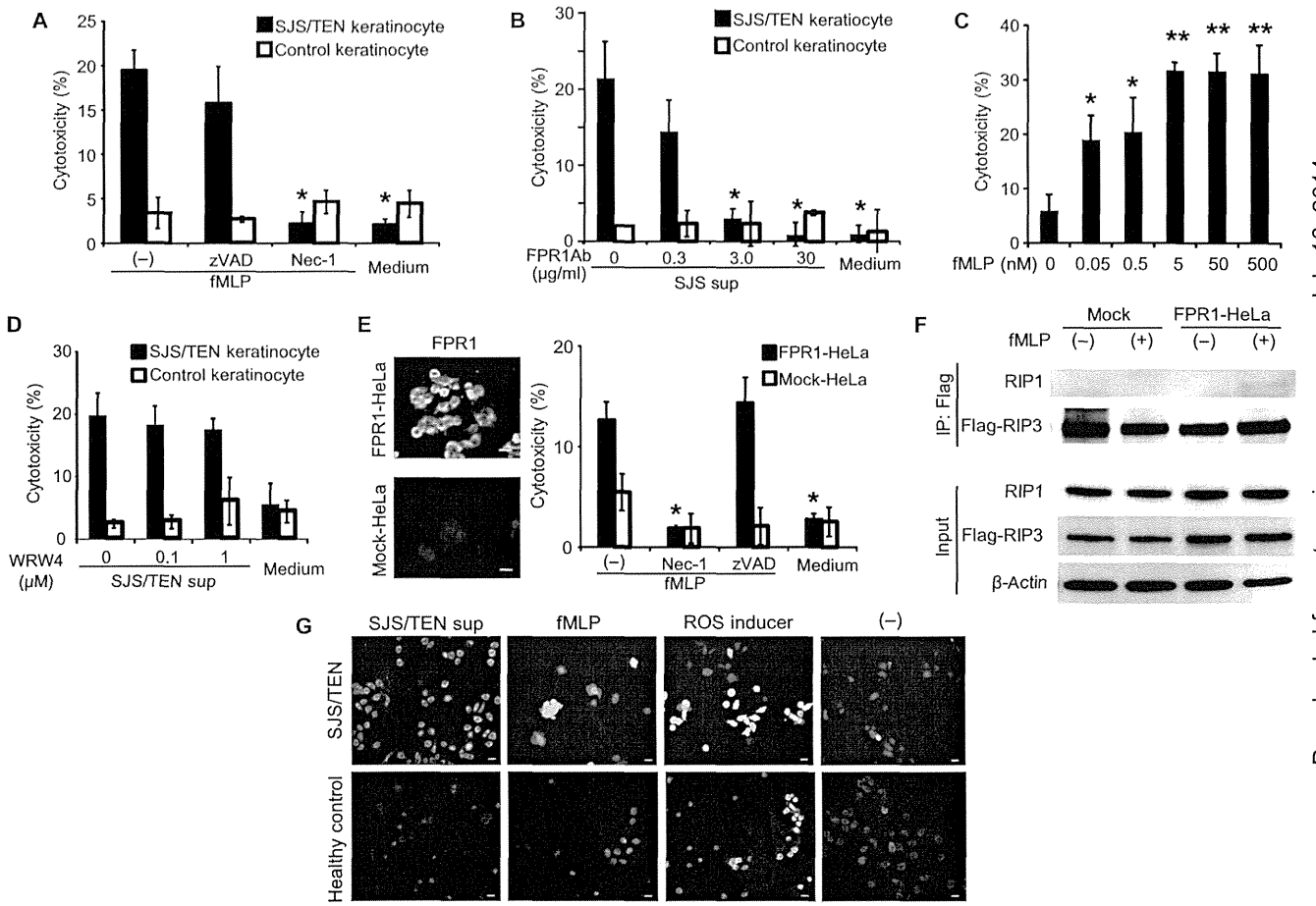

Fig. 6. FRP1 activation induces necrosis via the RIP1/RIP3 complex. (**A**) Effect of *f*MLP (5 nM) on cytotoxicity in the presence of zVAD (50 μM) or Nec-1 (50 μM) was analyzed using keratinocytes from SJS/TEN patients or healthy controls ($n = 4$). *$P < 0.05$. Keratinocytes were obtained from patient no. 10 (postlesional skin) and healthy control no. 5. (**B**) Effect of FPR1 neutralizing antibody on SJS/TEN PBMC supernatant–induced cytotoxicity was analyzed ($n = 4$). *$P < 0.01$. Keratinocytes were obtained from patient no. 10 and healthy control no. 5. PBMCs were obtained from patient no. 3 (postlesional skin). (**C**) Dose dependence of cytotoxicity by *f*MLP ($n = 4$). *$P < 0.05$; **$P < 0.01$. Keratinocytes were obtained from patient no. 3 (postlesional skin). (**D**) Effect of FPR2 antagonist (WRW4) on SJS/TEN PBMC supernatant cytotoxicity. Keratinocytes were preincubated with WRW4 for 15 min before exposure to SJS/TEN supernatant ($n = 5$). Keratinocytes were obtained from patient no. 10 (postlesional skin) and healthy control no. 7. PBMCs were obtained from patient no. 3 ($n = 4$). (**E**) Effect of necrosis and apoptosis inhibitors on cytotoxicity in FPR1-transfected, Flag-RIP3–expressing HeLa cells. Flag-RIP3–expressing HeLa cells were stably transfected with FPR1 and stimulated with *f*MLP, and cytotoxicity was assessed ($n = 4$). *$P < 0.01$ versus *f*MLP. (**F**) Immunoprecipitation of a Flag-tagged RIP3 pull-down from *f*MLP-exposed HeLa cells (FPR1-HeLa cells or mock-transfected HeLa cells). The experiments were repeated three times, and representative data are shown. (**G**) Representative images showing sensitivity of SJS/TEN keratinocytes to FPR1-induced ROS generation. SJS/TEN sup (25%), *f*MLP (500 nM), or ROS inducer (pyocyanin) (200 μM) was added to keratinocytes from SJS/TEN patients or healthy controls. After 30 min, ROS generation was measured. Scale bars, 5 μm. Keratinocytes were obtained from patient no. 3 (postlesional skin) and healthy control no. 6.

found that *f*MLP stimulation induced cytotoxicity only in FPR1-expressing RIP3-HeLa cells and not in mock-transfected cells (Fig. 6E). Although zVAD did not inhibit cytotoxicity, Nec-1 completely inhibited the effect. With *f*MLP stimulation, the RIP1/RIP3 complex was detected only in FRP1-expressing HeLa cells and not in mock-transfected HeLa cells (Fig. 5F). These data point to the conclusion that annexin A1 in the SJS/TEN supernatant is a potent activator of FPR1 and induces necroptosis in SJS/TEN keratinocytes.

The FPR1 signal induces the generation of reactive oxygen species (ROS) (*23*), which is also a mediator of necroptosis (*18*). Therefore, we investigated ROS generation in SJS/TEN supernatant–exposed keratinocytes. High levels of ROS generation were observed in SJS/TEN supernatant–exposed or *f*MLP-treated SJS/TEN keratinocytes examined by fluorescence microscopy, but not in control keratinocytes (Fig. 6G), indicating that SJS/TEN keratinocytes are sensitive to FPR1-induced ROS generation. Because FPR1 activates the MAP kinase cascade (*21*), we assessed the activation of MAP kinase in FPR1-expressing HeLa and mock-transfected HeLa cells. *f*MLP exposure did not induce the phosphorylation of c-Jun N-terminal kinase (JNK), p38, or ERK (extracellular signal–regulated kinase) (fig. S8).

Therapy for SJS/TEN model mice by necroptosis inhibitor

We administered a necroptosis blocker to our SJS/TEN model mice. NSA, which blocks necroptosis by inhibiting MLKL (*17*), prevents SJS/TEN supernatant–induced cytotoxicity in vitro (Fig. 7A). Whereas the vehicle-treated model mice showed marked conjunctival congestion and abundant cell death in their conjunctival epithelium, the NSA-treated mice showed no such reactions (Fig. 7B). We found numerous dead epithelial cells in the vehicle-treated model mice but not in the NSA-treated model mice (Fig. 7, C and D). Moreover, the vehicle-treated model mice showed RIP3 and FPR1 in conjunctiva similar to those seen in human SJS/TEN (Figs. 2D and 4E), whereas the NSA-treated model mice did not show these proteins in their conjunctiva (Fig. 7D).

DISCUSSION

Here, we show that necroptosis can be triggered by the interaction of annexin A1 and FPR1 and may contribute to the pathogenesis of SJS/TEN. Our data suggest that causative drug exposure induces annexin A1 secretion from monocytes in SJS/TEN patients. Annexin

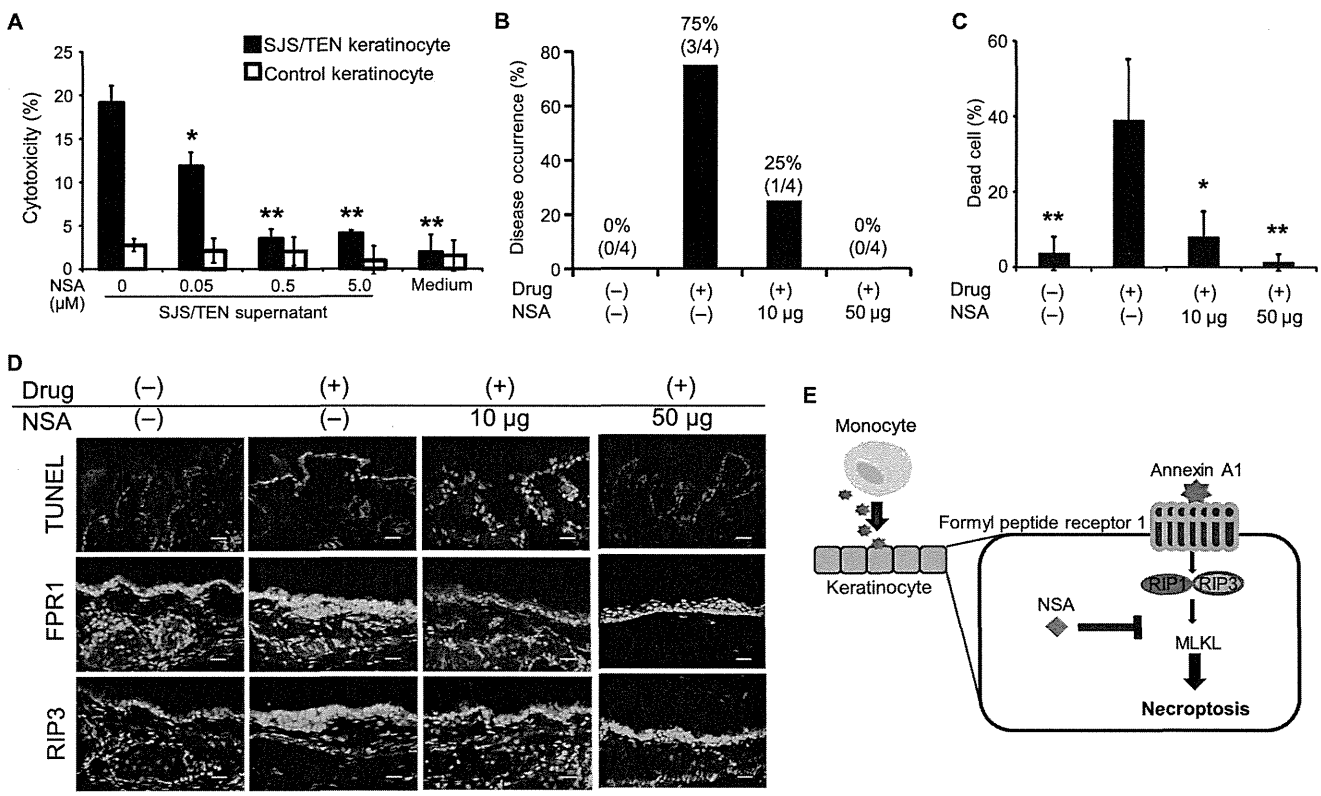

Fig. 7. Inhibition of necroptosis prevents SJS/TEN in model mice. (**A**) Effect of NSA on SJS/TEN supernatant–induced cytotoxicity ($n = 4$). *$P < 0.05$; **$P < 0.01$. Keratinocytes and PBMCs were obtained from patient no. 3 (postlesional skin). Keratinocytes were obtained from healthy control no. 4. (**B**) Model mice received NSA intraperitoneally, and eye abnormalities were scored as disease occurrence ($n = 4$). (**C**) Percentage of dead cells in conjunctiva epithelia was calculated ($n = 4$). *$P < 0.05$; **$P < 0.01$ versus Drug (+), NSA (–). (**D**) Using TUNEL (terminal deoxynucleotidyl transferase–mediated deoxyuridine triphosphate nick end labeling) assay, dead cells were visualized, and RIP3 and FPR1 expression was imaged in the conjunctiva of model mice. Nuclei were stained with PI. Representative images are shown. Scale bars, 10 μm. (**E**) Scheme of keratinocyte death mechanism. In SJS/TEN, the causative drug stimulates PBMCs (monocytes) to secrete annexin A1 (yellow star). The released annexin A1 binds to FPR1 and activates the necroptosis pathway through the RIP1/RIP3 complex. NSA, an MLKL inhibitor, can block necroptosis.

A1 in turn binds to FPR1 and induces FPR1 expression in keratinocytes, resulting in cell death via a necroptosis pathway (Fig. 7E).

Several stimulators of necroptosis, such as Fas and TNF-α, also stimulate apoptosis (*24*). Although it has been shown that artificial inhibition of casapse-8 or overexpression of RIP3 tends to induce necroptosis (*16*, *25*), it was not known whether these imbalances also occur naturally. Our present data show that necroptosis signaling by annexin A1/FRP1 does not appear to overlap with apoptosis. To induce keratinocyte necroptosis, both annexin A1 and FPR1 are required. We show that annexin A1 induces FPR1 expression in SJS/TEN keratinocytes. Therefore, keratinocyte necroptosis may occur only when annexin A1 is up-regulated, namely, under conditions of drug allergy.

Several mediators of SJS/TEN have been proposed, such as Fas ligand (*5*), soluble Fas ligand (*26*), perforin, granzyme B (*27*), and granulysin (*2*, *28*). For example, granulysin was identified by DNA microarray of SJS/TEN bullae cells; the data showed the mRNA of granulysin to be elevated, as well as the mRNAs of other proapoptotic molecules, such as FasL, perforin, and granzyme B (*2*). These results suggest that several pathways are activated in apoptosis in vivo.

It is not clear why these "cell death mediators" affect skin and result in widespread mucocutaneous erosions in SJS/TEN but not in ODSR, and whether there are individual differences in proapoptotic molecule expression is unknown. In this regard, inducible FPR1 expression levels differ greatly between SJS/TEN and ODSR (Fig. 5, A and B), suggesting that inducible FPR1 expression levels may determine SJS/TEN or ODSR occurrence and regulate the necroptosis that is seen in SJS/TEN.

Although there are no genetic differences in FPR1 promoters among SJS/TEN patients, ODSR patients, and healthy controls (data file S1), annexin A1–FRP1 are candidate markers of disease occurrence and may be promising therapeutic targets. In addition, necroptosis is a potential drug target for SJS/TEN treatment, and NSA is a therapeutic candidate.

MATERIALS AND METHODS

Study design

For the human sample studies, skin PBMCs and sera from healthy controls and SJS/TEN or ODSRs patients (table S2) were obtained from Hokkaido University Hospital. The collection of samples was approved by the local ethics committee and the institutional review board of Hokkaido University. To investigate SJS/TEN pathogenesis, approval was given for the collection of blood, serum, and skin samples. We also explained the potential side effects of skin biopsy to the patients. After we obtained the informed consent of the patient, we obtained the blood, serum, and skin samples in the acute phase of the disease and in the resolution phase.

The mouse studies were performed under a protocol approved by the ethical committee for animal studies of Hokkaido University. Immunocompromised NOG mice at 6 to 7 weeks of age were purchased from Jackson Laboratory.

Immunohistochemistry

The following primary antibodies were used: RIP3 (Abcam) and FPR1 (LifeSpan). Anti–annexin A1 antibody was generated by peptide immunization of rabbits, as was rabbit polyclonal antibody to the synthetic peptide MAMVSEFLKQAWF, corresponding to amino acid residues 1 to 13 in annexin A1. These antibodies were generated at our request by Hokudo Co. Ltd.

Electron microscopy

Skin sections were fixed by the dropwise addition of glutaraldehyde and were analyzed according to standard methods. Necrotic and apoptotic cells were counted in all keratinocytes (N = 80) in the SJS/TEN lesions.

The morphological changes in supernatant-treated keratinocytes by electron microscopy were examined. Necrotic and apoptotic cells were counted among dead keratinocytes (n = 35).

ELISPOT IFN-γ assay

PBMCs were prepared from patients' blood and isolated by Ficoll-Isopaque (Pharmacia Fine Chemicals) density gradient centrifugation. The number of IFN-γ–producing cells was determined with an ELISPOT assay kit (Human IFN-γ ELISPOT PVDF-Enzymatic; Diaclone). The number of spots was counted under a dissecting microscope (SMZ1500; Nikon).

Supernatant

PBMCs were obtained from SJS/TEN or ODSRs patients. $CD14^+$ and $CD8^+$ cell depletions were performed with magnetic-activated cell sorting (MACS; Miltenyi Biotec). Isolated cells were exposed to causative drugs and then cultured for 5 days to allow proliferation of drug-specific T cells. The cells were stimulated by reexposure with same causative drugs for 1 day, and then supernatant was collected. Drug concentration was determined from the data of a lymphocyte transformation test (*29*). In some experiments, PBMCs were incubated with several concentrations of causative drug for 5 days. [^{3}H]Thymidine (1 μCi) was added for the last 12 hours. Causative drug–specific proliferation was determined by measuring [^{3}H]thymidine incorporation. The results were expressed as stimulation indices (SI): (cpm in cultures + drug)/(cpm in cultures without drug). The concentration with the highest SI was chosen for further experiments.

Keratinocyte culture

Primary keratinocytes were isolated from patients, cultured and then expanded in CnT-57 from CELLnTEC, and used for the assay with no more than four passages. The keratinocytes were incubated with CnT-57 in a 5% CO_2 incubator at 37°C.

Cytotoxic assays

Cultured keratinocytes were added to the supernatant of the causative drug–exposed PBMCs. In some experiments, zVAD (R&D Systems) or Nec-1 (Enzo Life Sciences) was preincubated with the cells for 1 hour before supernatant addition. *f*MLP and Ac2-26 were purchased from Sigma-Aldrich. Anti–MHC I antibody (W6/32) was purchased from BioLegend. FPR2 antagonist (WRW4) was purchased from Tocris Bioscience. At 8 or 16 hours, the cytotoxicity was analyzed with an LDH (lactate dehydrogenase) assay (R&D Systems) and/or trypan blue staining (R&D Systems). The data were comparable with LDH or trypan blue staining assays (fig. S9). All experiments were repeated at least three times.

siRNA transfection

For transient knockdown, keratinocytes were transfected on two consecutive days with nontargeting RNA duplexes or duplexes targeting RIP3 (siRNA-1: GAACUGUUUGUUAACGCAA and siRNA-2: GGCAAGUCUGGAUAACGA), and control siRNA duplex (that is, a scrambled siRNA with a sequence that matched no known mRNA sequence in the vertebrate genome) (Ambion) using Lipofectamine RNAiMAX (Invitrogen). At 48 hours, cells were used in experiments.

Mass spectrometry (LC-MS/MS)

The proteins in SJS/TEN supernatant were identified by mass spectrometry analysis as described (*30*). The primary ion spectrum data generated by LC-MS/MS were screened against International Protein Index human protein databases with the Mascot program (Matrix Science) to identify high-scoring proteins.

Removal of annexin A1 from supernatant

Supernatant was mixed with the anti–annexin A1 antibody and gently mixed at 4°C overnight. Protein G Dynabeads (Dynal) were then added to the mixture, followed by 2 hours of rotation at 4°C. Annexin A1 could not be detected in annexin A1–depleted SJS/TEN supernatant with annexin A1 peptide ELISA.

Annexin A1 peptide ELISA

Rabbit polyclonal antibody against annexin A1 peptide (amino acids 1 to 13) was used for annexin A1 peptide ELISA to measure annexin A1 concentration.

Samples were added to the wells of a microplate. After overnight incubation at 4°C, rabbit polyclonal antibody against annexin A1 peptide (amino acids 1 to 13) (1: 5000) was added, followed by β-galactosidase anti-rabbit IgG antibody (1:2000). The fluorescence was measured with a microplate reader.

FPR1-expressing stable cell lines

3xFlag-RIP3-HeLa cells were established as described (*17*). Normal human full-length FRP1 cDNA (complementary DNA) was synthesized by Integrated DNA Technologies Inc. and subcloned into the Xho I and Kpn I sites of pcDNA3.1/Zeo vector (Invitrogen). RIP3-HeLa cells were transfected with pcDNA3.1/Zeo plasmid encoding FRP1 with FuGENE 6 (Roche) and were selected with Zeocin (100 μg/ml) (Invitrogen).

Immunoprecipitation

The cells were lysed for 30 min on ice in a lysis buffer. Cell lysate was spun at 15,000 rpm for 10 min, and the soluble fraction was collected. One milligram of extracted protein in lysis buffer was immunoprecipitated for 2 hours with anti-FLAG M2 affinity gel (Sigma-Aldrich) at 4°C. The immunoprecipitates were washed five times with lysis buffer. The beads were eluted with the corresponding antigenic peptide (250 μg/ml).

FPR1-induced ROS generation

SJS/TEN supernatant (25%), *f*MLP (500 nM), or ROS inducer (pyocyanin) (200 μM) was added to keratinocytes from SJS/TEN patients or healthy controls. After 30 min, ROS generation was detected by using the Total ROS Detection Kit (Enzo Life Sciences).

Treatment of necroptosis inhibitor for SJS/TEN model mice

Patient PBMCs (2×10^6) were injected intravenously into immunocompromised NOG mice, followed by oral administration of a causative drug for 12 days (*15*). NSA (10 or 50 μg) (provided by L. Sun and X. Wang) or DMSO was also administered intraperitoneally to mice daily. The mice were observed for manifestations of eye disease.

Terminal deoxynucleotidyl transferase–mediated deoxyuridine triphosphate nick end labeling

To detect dead cells by DNA fragmentation by labeling the terminal end of nucleic acids, a TUNEL assay was performed according to the manufacturer's protocol (Takara Bio).

Statistics

In all figures, data are presented as means ± SD of at least three independent experiments. *P* values were calculated with one-way analysis of variance (ANOVA) and two-tailed independent Student's *t* tests, and $P < 0.05$ was considered significant.

SUPPLEMENTARY MATERIALS

www.sciencetranslationalmedicine.org/cgi/content/full/6/245/245ra95/DC1
Fig. S1. Causative drug-specific lymphocytes in patients' peripheral blood.
Fig. S2. The cytotoxicity of supernatant from DIHS/DRESS PBMCs.
Fig. S3. The cytotoxicity of supernatant from irrelevant drug–exposed SJS/TEN PBMCs.
Fig. S4. The cytotoxicity of keratinocytes from normal-appearing postlesional skin and nonlesional skin.
Fig. S5. Protein levels of necroptosis signaling molecules in keratinocytes from SJS/TEN patients, ODSR patients, or healthy controls.
Fig. S6. Effect of poly(I:C), TNF-α, and granulysin on SJS/TEN keratinocyte cytotoxicity.
Fig. S7. The cytotoxicity of $CD14^{bright}$ $CD16^{-}$ and $CD14^{dim}$ $CD16^{+}$ cells on SJS/TEN keratinocytes.
Fig. S8. FPR1 stimulation does not induce phosphorylation of JNK, p38, or ERK.
Fig. S9. Cytotoxicity in SJS/TEN keratinocytes, ODSR keratinocytes, or healthy control keratinocytes induced by PBMC supernatant, as measured by LDH assay.
Table S1. Mass spectrometry result of the proteins in SJS/TEN supernatant.
Table S2. Patient and healthy control information.
Data File S1. The promoter region of FPR1 has no pathogenic mutations.
Reference (*31*)

REFERENCES AND NOTES

1. A. Downey, C. Jackson, N. Harun, A. Cooper, Toxic epidermal necrolysis: Review of pathogenesis and management. *J. Am. Acad. Dermatol.* **66**, 995–1003 (2012).
2. W.H. Chung, S. I. Hung, J. Y. Yang, S. C. Su, S. P. Huang, C. Y. Wei, S. W. Chin, C. C. Chiou, S. C. Chu, H. C. Ho, C. H. Yang, C. F. Lu, J. Y. Wu, Y. D. Liao, Y. T. Chen, Granulysin is a key mediator for disseminated keratinocyte death in Stevens-Johnson syndrome and toxic epidermal necrolysis. *Nat. Med.* **14**, 1343–1350 (2008).
3. T. Hanafusa, H. Azukizawa, S. Matsumura, I. Katayama, The predominant drug-specific T-cell population may switch from cytotoxic T cells to regulatory T cells during the course of anticonvulsant-induced hypersensitivity. *J. Dermatol. Sci.* **65**, 213–219 (2012).
4. W. H. Chung, S. I. Hung, Recent advances in the genetics and immunology of Stevens-Johnson syndrome and toxic epidermal necrosis. *J. Dermatol. Sci.* **66**, 190–196 (2012).
5. I. Viard, P. Wehrli, R. Bullani, P. Schneider, N. Holler, D. Salomon, T. Hunziker, J. H. Saurat, J. Tschopp, L. E. French, Inhibition of toxic epidermal necrolysis by blockade of CD95 with human intravenous immunoglobulin. *Science* **282**, 490–493 (1998).
6. P. Golstein, G. Kroemer, Cell death by necrosis: Towards a molecular definition. *Trends Biochem. Sci.* **32**, 37–43 (2007).
7. A. Kawahara, T. Kobayashi, S. Nagata, Inhibition of Fas-induced apoptosis by Bcl-2. *Oncogene* **17**, 2549–2554 (1998).
8. D. Vercammen, P. Vandenabeele, R. Beyaert, W. Declercq, W. Fiers, Tumour necrosis factor-induced necrosis versus anti-Fas-induced apoptosis in L929 cells. *Cytokine* **9**, 801–808 (1997).
9. A. Degterev, Z. Huang, M. Boyce, Y. Li, P. Jagtap, N. Mizushima, G. D. Cuny, T. J. Mitchison, M. A. Moskowitz, J. Yuan, Chemical inhibitor of nonapoptotic cell death with therapeutic potential for ischemic brain injury. *Nat. Chem. Biol.* **1**, 112–119 (2005).
10. A. Degterev, J. Hitomi, M. Germscheid, I. L. Ch'en, O. Korkina, X. Teng, D. Abbott, G. D. Cuny, C. Yuan, G. Wagner, S. M. Hedrick, S. A. Gerber, A. Lugovskoy, J. Yuan, Identification of RIP1 kinase as a specific cellular target of necrostatins. *Nat. Chem. Biol.* **4**, 313–321 (2008).
11. P. S. Welz, A. Wullaert, K. Vlantis, V. Kondylis, V. Fernández-Majada, M. Ermolaeva, P. Kirsch, A. Sterner-Kock, G. van Loo, M. Pasparakis, FADD prevents RIP3-mediated epithelial cell necrosis and chronic intestinal inflammation. *Nature* **477**, 330–334 (2011).
12. C. Günther, E. Martini, N. Wittkopf, K. Amann, B. Weigmann, H. Neumann, M. J. Waldner, S. M. Hedrick, S. Tenzer, M. F. Neurath, C. Becker, Caspase-8 regulates TNF-α-induced epithelial necroptosis and terminal ileitis. *Nature* **477**, 335–339 (2011).
13. A. Beeler, O. Engler, B. O. Gerber, W. J. Pichler, Long-lasting reactivity and high frequency of drug-specific T cells after severe systemic drug hypersensitivity reactions. *J. Allergy Clin. Immunol.* **117**, 455–462 (2006).
14. A. Rozieres, A. Hennino, K. Rodet, M. C. Gutowski, N. Gunera-Saad, F. Berard, G. Cozon, J. Bienvenu, J. F. Nicolas, Detection and quantification of drug-specific T cells in penicillin allergy. *Allergy* **64**, 534–542 (2009).

15. N. Saito, N. Yoshioka, R. Abe, H. Qiao, Y. Fujita, D. Hoshina, A. Suto, S. Kase, N. Kitaichi, M. Ozaki, H. Shimizu, Stevens-Johnson syndrome/toxic epidermal necrolysis mouse model generated by using PBMCs and the skin of patients. *J. Allergy Clin. Immunol.* **131**, 434–441.e9 (2013).
16. D. W. Zhang, J. Shao, J. Lin, N. Zhang, B. J. Lu, S. C. Lin, M. Q. Dong, J. Han, RIP3, an energy metabolism regulator that switches TNF-induced cell death from apoptosis to necrosis. *Science* **325**, 332–336 (2009).
17. L. Sun, H. Wang, Z. Wang, S. He, S. Chen, D. Liao, L. Wang, J. Yan, W. Liu, X. Lei, X. Wang, Mixed lineage kinase domain-like protein mediates necrosis signaling downstream of RIP3 kinase. *Cell* **148**, 213–227 (2012).
18. Z. Wang, H. Jiang, S. Chen, F. Du, X. Wang, The mitochondrial phosphatase PGAM5 functions at the convergence point of multiple necrotic death pathways. *Cell* **148**, 228–243 (2012).
19. M. Perretti, F. D'Acquisto, Annexin A1 and glucocorticoids as effectors of the resolution of inflammation. *Nat. Rev. Immunol.* **9**, 62–70 (2009).
20. M. Tohyama, H. Watanabe, S. Murakami, Y. Shirakata, K. Sayama, M. Iijima, K. Hashimoto, Possible involvement of CD14+ CD16+ monocyte lineage cells in the epidermal damage of Stevens–Johnson syndrome and toxic epidermal necrolysis. *Br. J. Dermatol.* **166**, 322–330 (2012).
21. S. D. Kim, J. M. Kim, S. H. Jo, H. Y. Lee, S. Y. Lee, J. W. Shim, S. K. Seo, J. Yun, Y. S. Bae, Functional expression of formyl peptide receptor family in human NK cells. *J. Immunol.* **183**, 5511–5517 (2009).
22. G. Leoni, A. Alam, P. A. Neumann, J. D. Lambeth, G. Cheng, J. McCoy, R. S. Hilgarth, K. Kundu, N. Murthy, D. Kusters, C. Reutelingsperger, M. Perretti, C. A. Parkos, A. S. Neish, A. Nusrat, Annexin A1, formyl peptide receptor, and NOX1 orchestrate epithelial repair. *J. Clin. Invest.* **123**, 443–454 (2013).
23. C. C. Wentworth, A. Alam, R. M. Jones, A. Nusrat, A. S. Neish, Enteric commensal bacteria induce extracellular signal-regulated kinase pathway signaling via formyl peptide receptor-dependent redox modulation of dual specific phosphatase 3. *J. Biol. Chem.* **286**, 38448–38455 (2011).
24. P. Vandenabeele, L. Galluzzi, T. Vanden Berghe, G. Kroemer, Molecular mechanisms of necroptosis: An ordered cellular explosion. *Nat. Rev. Mol. Cell Biol.* **11**, 700–714 (2010).
25. M. A. O'Donnell, E. Perez-Jimenez, A. Oberst, A. Ng, R. Massoumi, R. Xavier, D. R. Green, A. T. Ting, Caspase 8 inhibits programmed necrosis by processing CYLD. *Nat. Cell Biol.* **13**, 1437–1442 (2011).
26. R. Abe, T. Shimizu, A. Shibaki, H. Nakamura, H. Watanabe, H. Shimizu, Toxic epidermal necrolysis and Stevens-Johnson syndrome are induced by soluble Fas ligand. *Am. J. Pathol.* **162**, 1515–1520 (2003).
27. S. J. Posadas, A. Padial, M. J. Torres, C. Mayorga, L. Leyva, E. Sanchez, J. Alvarez, A. Romano, C. Juarez, M. Blanca, Delayed reactions to drugs show levels of perforin, granzyme B, and Fas-L to be related to disease severity. *J. Allergy Clin. Immunol.* **109**, 155–161 (2002).
28. R. Abe, N. Yoshioka, J. Murata, Y. Fujita, H. Shimizu, Granulysin as a marker for early diagnosis of the Stevens–Johnson syndrome. *Ann. Intern. Med.* **151**, 514–515 (2009).
29. G. Porebski, T. Pecaric-Petkovic, M. Groux-Keller, M. Bosak, T. T. Kawabata, W. J. Pichler, In vitro drug causality assessment in Stevens–Johnson syndrome—Alternatives for lymphocyte transformation test. *Clin. Exp. Allergy* **43**, 1027–1037 (2013).
30. R. S. Nozawa, K. Nagao, H. T. Masuda, O. Iwasaki, T. Hirota, N. Nozaki, H. Kimura, C. Obuse, Human POGZ modulates dissociation of HP1α from mitotic chromosome arms through Aurora B activation. *Nat. Cell Biol.* **12**, 719–727 (2010).
31. H. M. Miettinen, Regulation of human formyl peptide receptor 1 synthesis: Role of single nucleotide polymorphisms, transcription factors, and inflammatory mediators. *PLOS One* **6**, e28712 (2011).

Acknowledgments: We thank. M. Kagaya-Takehara and A. Moriya for their technical expertise, and H. Takahashi and S. Hatakeyama for their technical advice. Flag-RIP3-HeLa cells were donated by L. Sun and X. Wang. **Funding:** This work was supported in part by a Health and Labor Sciences Research Grant from the Ministry of Health, Labor, and Welfare of Japan (Research on Development of New Drugs; H24-Bio-001 to R.A.) and a Grant-in-Aid for Scientific Research from the Ministry of Education, Culture, Sports, Science and Technology of Japan (no. 24390275 to R.A.). **Author contributions:** N.S. conceived the study, designed the experiments, wrote the paper, and performed most of the experiments with help from H.Q., T.Y., K. Nishimura, A.S., Y.F., and H.N.; R.A. conceived the study, designed the experiments, and wrote the paper; H.S. analyzed results and wrote the paper; S. Shinkuma generated FRP1-expressing HeLa cells; S. Suzuki and T.N. performed the mutation search in the FPR1 promoter region; and K. Nagao and C.O. performed mass spectrometry (LC-MS/MS). **Competing interests:** The authors declare that they have no competing interests.

Submitted 10 December 2013
Accepted 27 May 2014
Published 16 July 2014
10.1126/scitranslmed.3008227

Citation: N. Saito, H. Qiao, T. Yanagi, S. Shinkuma, K. Nishimura, A. Suto, Y. Fujita, S. Suzuki, T. Nomura, H. Nakamura, K. Nagao, C. Obuse, H. Shimizu, R. Abe, An annexin A1–FPR1 interaction contributes to necroptosis of keratinocytes in severe cutaneous adverse drug reactions. *Sci. Transl. Med.* **6**, 245ra95 (2014).

Hepatology Research

Hepatology Research 2014 doi: 10.1111/hepr.12421

Original Article

Serum granulysin levels as a predictor of serious telaprevir-induced dermatological reactions

Goki Suda,[1] Yoshiya Yamamoto,[2] Astushi Nagasaka,[3] Ken Furuya,[4] Mineo Kudo,[5] Yoshimichi Chuganji,[6] Yoko Tsukuda,[1] Seiji Tsunematsu,[1] Fumiyuki Sato,[1] Katsumi Terasita,[1] Masato Nakai,[1] Hiromasa Horimoto,[1] Takuya Sho,[1] Mitsuteru Natsuizaka,[1] Kouji Ogawa,[1] Shunsuke Ohnishi,[1] Makoto Chuma,[1] Yasuyuki Fujita,[7] Riichiro Abe,[7] Miki Taniguchi,[8] Mina Nakagawa,[8] Yasuhiro Asahina[8] and Naoya Sakamoto[1] for the NORTE Study Group

[1]Department of Gastroenterology and Hepatology, Graduate School of Medicine, Hokkaido University, [2]Hakodate City Hospital, [3]Sapporo City General Hospital, [4]Hokkaido Social Insurance Hospital, [5]Sapporo Hokuyu Hospital, [7]Department of Dermatology, Hokkaido University Graduate School of Medicine, Hokkaido, [6]Tokyo Metropolitan Bokuto Hospital, and [8]Department of Gastroenterology and Hepatology, Tokyo Medical and Dental University, Tokyo, Japan

Aim: Telaprevir-based therapy for chronic hepatitis C patients is effective; however, the high prevalence of dermatological reactions is an outstanding issue. The mechanism and characteristics of such adverse reactions are unclear; moreover, predictive factors remain unknown. Granulysin was recently reported to be upregulated in the blisters of patients with Stevens–Johnson syndrome (SJS). Therefore, we investigated the risk factors for severe telaprevir-induced dermatological reactions as well as the association between serum granulysin levels and the severity of such reactions.

Methods: A total of 89 patients who received telaprevir-based therapy and had complete clinical information were analyzed. We analyzed the associations between dermatological reactions and clinical factors. Next, we investigated the time-dependent changes in serum granulysin levels in five and 14 patients with grade 3 and non-grade 3 dermatological reactions, respectively.

Results: Of the 89 patients, 57 patients had dermatological reactions, including nine patients with grade 3. Univariate analysis revealed that grade 3 dermatological reactions were significantly associated with male sex. Moreover, serum granulysin levels were significantly associated with the severity of dermatological reactions. Three patients with grade 3 dermatological reaction had severe systemic manifestations including SJS, drug-induced hypersensitivity syndrome, and systemic lymphoid swelling and high-grade fever; all were hospitalized. Importantly, among the three patients, two patients' serum granulysin levels exceeded 8 ng/mL at onset and symptoms deteriorated within 6 days.

Conclusion: Male patients are at high risk for severe telaprevir-induced dermatological reactions. Moreover, serum granulysin levels are significantly associated with the severity of dermatological reactions and may be a predictive factor in patients treated with telaprevir-based therapy.

Key words: drug-induced hypersensitivity syndrome, granulysin, hepatitis C virus, telaprevir, toxic epidermal necrolysis

INTRODUCTION

HEPATITIS C IS a major pathogen causing liver cirrhosis and hepatocellular carcinoma worldwide. Until recently, standard therapies for chronic hepatitis C virus (HCV) genotype 1 infection were based on the combination of pegylated interferon (PEG IFN) and ribavirin (RBV); these combination therapies yield a sustained virological response (SVR) rate of approximately 50%.[1] Several classes of novel direct-acting antivirals

Correspondence: Dr Goki Suda, Department of Gastroenterology and Hepatology/Graduate School of Medicine, Hokkaido University, North 15, West 7, Kita-ku, Sapporo, Hokkaido 060-8638, Japan. Email: gsudgast@pop.med.hokudai.ac.jp

Conflict of interest: The authors declare that they have nothing to disclose regarding funding from the industry or conflicts of interest with respect to the manuscript.

Received 9 June 2014; revision 27 August 2014; accepted 4 September 2014.

(DAA) were recently developed and tested in clinical trials. Two first-generation HCV NS3/4A protease inhibitors, boceprevir[2,3] and telaprevir,[4–6] have been approved for the treatment of genotype 1 HCV infection. The inclusion of these agents in HCV treatment regimens has led to large improvements in treatment success rates.

Telaprevir, the first DAA, is administrated in combination with PEG IFN and RBV for 24 weeks, resulting in SVR rates up to 70–80%.[4,6–8] Although the telaprevir combination regimen is highly effective, the high frequency and severity of adverse events are outstanding issues limiting its use. Dermatological reactions are particularly prevalent, developing in 56–84.6% of patients treated with telaprevir, PEG IFN and RBV combination therapy.[9,10] Moreover, the prevalence of severe dermatological reactions including Stevens–Johnson syndrome/toxic epidermal necrolysis (SJS/TEN) and drug-induced hypersensitivity syndrome (DIHS) are substantially higher in patients treated with telaprevir-based therapy than PEG IFN and RBV combination therapy.[8,10] McHutchison *et al.* reported that 7% of patients treated with telaprevir, PEG IFN and RBV combination therapy discontinue therapy because of rash or pruritus in contrast to only 1% of patients treated with PEG IFN and RBV.[8] In some patients, serious skin reactions persist even after stopping all drugs.[10] However, the pathogenesis and clinical predictors of these adverse reactions are poorly understood.

Granulysin is a 15-kDa cationic cytolytic protein released by cytotoxic T lymphocytes and natural killer cells that induces apoptosis in target cells and has antimicrobial activities.[11] Serum levels of granulysin are elevated in primary virus infections including Epstein–Barr virus and parvovirus B19.[12] It was recently reported that serum granulysin levels are significantly elevated in patients with several types of severe dermatological lesions including SJS/TEN, which is the characteristic serious adverse event in telaprevir-containing regimens.[13,14]

Accordingly, the present study determined the risk factors for severe dermatological reactions in patients receiving telaprevir, PEG IFN and RBV combination therapy as well as the association between serum levels of granulysin and severe dermatological reactions.

METHODS

Patients and methods

IN THIS RETROSPECTIVE case–control study, at Hokkaido University Hospital and associated hospitals in the NORTE Study Group, between December 2011 and November 2013, a total of 123 patients positive for HCV genotype 1 with high serum HCV RNA titer (>5 log IU/mL) received PEG IFN, RBV and telaprevir combination therapy. Patients were excluded if they required hemodialysis or had a positive test result for serum hepatitis B surface antigen, co-infection with other HCV genotypes or HIV, evidence of autoimmune hepatitis or alcoholic hepatitis, or malignancy. Serum granulysin levels were analyzed in five healthy volunteers with no HCV, HIV or hepatitis B virus infection or any inflammatory diseases.

Written informed consent according to the process approved by the hospital's ethics committee was obtained from each patient. The study protocol conformed to the ethical guidelines of the Declaration of Helsinki and was approved by the ethics committee of each participating hospital.

Study design and treatment regimen

Telaprevir 500 or 750 mg was typically administrated every 8 h after meals for 12 weeks. PEG IFN-α-2b (PegIntron; MSD, Tokyo, Japan) 1.5 IU/kg was administrated s.c. once per week for 24 weeks. RBV (Rebetol; MSD) was administrated for 24 weeks in two divided daily doses according to bodyweight: 600, 800 and 1000 mg for patients with bodyweights of less than 60, 60–80 and more than 80 kg, respectively. The doses of PEG IFN-α-2b, RBV and telaprevir were reduced at the attending physician's discretion on the basis of hemoglobin levels, decreased white blood cell or platelet counts, or adverse events.

During treatment, patients were assessed as outpatients at weeks 1, 2, 4, 6 and 8, and then every 4 weeks thereafter for the duration of treatment. Physical examinations and blood tests were performed at all time points.

Outcomes

The primary end-point was SVR, which was defined as undetectable serum HCV RNA at 24 weeks after the end of treatment. The secondary end-points were end-of-treatment virological responses (HCV RNA undetectable in serum) and rapid virological response (RVR), which was defined as undetectable serum HCV RNA at 4 weeks after the start of treatment. Dermatological reactions were classified according to severity in the same manner as in phase III trials in Japan.[10]

Serum granulysin measurement

To evaluate serum granulysin levels in chronic hepatitis C, we first measured serum granulysin levels in five

healthy volunteers and compared them with those of 20 chronic hepatitis C patients before treatment. Serum granulysin levels were measured at the onset of dermatological reactions (within 3 days of onset); if the symptoms worsened, the time when worsening occurred was adopted. Meanwhile, in patients with no dermatological reactions, the highest serum granulysin level during treatment was adopted.

Serum granulysin levels were measured by a sandwich enzyme-linked immunosorbent assay as described previously.[12,14,15] Briefly, plates coated with 5 mg/mL mouse antibody against human granulysin, RB1 antibody, were washed with phosphate-buffered saline containing 0.1% Tween-20. Next, they were blocked with 10% fetal bovine serum in washing buffer at room temperature for 2 h. The samples and standards (Recombinant Granulysin; R&D Systems, Minneapolis, MN, USA) were incubated for 2 h at room temperature. Next, they were reacted with 0.1 mg/mL biotinylated mouse antibody against human granulysin, RC8 antibody. The plates were subsequently treated with horseradish peroxidase-conjugated streptavidin (Roche Diagnostics, Basel, Switzerland). The plates were then incubated with tetramethyl-benzidine substrate (Sigma, St Louis, MO, USA), and 1 M sulfuric acid was then added. The optical density was measured at 450 nm using a microplate reader.

Diagnosis of dermatological reactions

Dermatological reactions were investigated throughout the 24-week administration period in the telaprevir-based combination therapy. Dermatological reactions were classified according to severity as follows. Grade 1 was defined as involvement of less than 50% of the body surface and no evidence of systemic symptoms. Grade 2 was defined as involvement of less than 50% of the body surface but with multiple or diffuse lesions or rashes with characteristic mild systemic symptoms or mucous membrane involvement with no ulceration/erosion. Grade 3 was defined as a generalized rash involving 50% or more of the body surface or a rash with any new significant systemic symptoms and considered to be related to the onset and/or progression of the rash. Life-threatening reactions included SJS, TEN, drug rash with eosinophilia and systemic symptoms (DRESS)/DIHS, erythema multiforme and other life-threatening symptoms, or patients presenting with features of serious disease.

When adverse skin reactions were detected, the attending physician classified the degree of severity and referred the patients to a dermatologist as needed. In principal, when grade 3 dermatological reactions occurred, the attending physician referred the patient to a dermatologist and discontinued telaprevir. When severe dermatological reactions including SJS/TEN and DRESS/DIHS were suspected, all drugs were discontinued immediately. SJS/TEN and DIHS were diagnosed by skin biopsy and according to disease criteria, respectively.

Statistical analysis

Categorical and continuous variables were analyzed by the χ^2-test and the unpaired Mann–Whitney *U*-test, respectively. All *P*-values were two-tailed, and the level of significance was set at $P < 0.05$. Multivariate logistic regression analysis with stepwise forward selection included variables showing $P < 0.05$ in univariate analyses.

The association between dermatological reactions and serum granulysin levels were evaluated by one-way ANOVA followed by Tukey's honestly significant difference test. All statistical analyses were performed using SPSS version 21.0 (IBM Japan, Tokyo, Japan).

RESULTS

Patients

WE INCLUDED 123 chronic hepatitis C patients who received telaprevir-based triple therapy. Of these, 89 patients who had proper information of dermatological adverse events were included. The baseline characteristics of patients are shown in Table 1.

Of these 89 patients, time-dependent changes of serum granulysin concentrations were measured in 20 who had had conserved serum, at least, at the pretreatment point, 1 and 2 weeks after commencement of therapy, 1 and 2 months after commencement of therapy, the onset point of dermatological adverse reaction and the worsening point if symptoms became worse.

Among the 89 patients, 64% (57/89) developed dermatological reactions, including nine with grade 3 reactions (Table 2). The characteristics of dermatological reactions by grade are shown in Table 2. Non-grade 3 dermatological reactions tended to occur early during treatment compared to grade 3 dermatological reactions.

Association between dermatological reactions and treatment outcomes

First, we determined whether dermatological reactions were associated with final treatment outcomes.

Table 1 Baseline characteristics of the participating patients

Total number	89
HCV genotype 1b (1b/others)	89/0
Age (years)†	60.0 (19–73)
Sex (male/female)	48/41
Bodyweight (kg)†	63.0 (32–97)
Baseline white blood cell count (/μL)†	4800 (1500–9800)
Baseline hemoglobin level (g/dL)†	13.5 (9.9–16.7)
Baseline platelet count ($\times 10^3$)†	15.9 (6.6–86)
Baseline ALT level (IU/L)†	40 (15–300)
Baseline HCV RNA level ($\log^{10}$ IU/mL)†	6.5 (3.2–7.6)
Initial telaprevir dose (1500/2250 mg)	20/89
Initial PEG IFN dose (1.5/<1.5 μg/kg)	775/14
Initial RBV dose (mg/kg)†	9.8 (2.2–15.5)
IL28B gene (rs8099917) (TT/non-TT/ ND)	51/22/16
HCV 70 core mutation (wild/ mutant/ND)	43/24/22
Previous treatment (naïve/relapse/NVR)	40/38/11

†Data are shown as median (range) values.
ALT, alanine transaminase; HCV, hepatitis C virus; IL28B, interleukin 28B; ND, not done; PEG IFN, pegylated interferon; RBV, ribavirin.

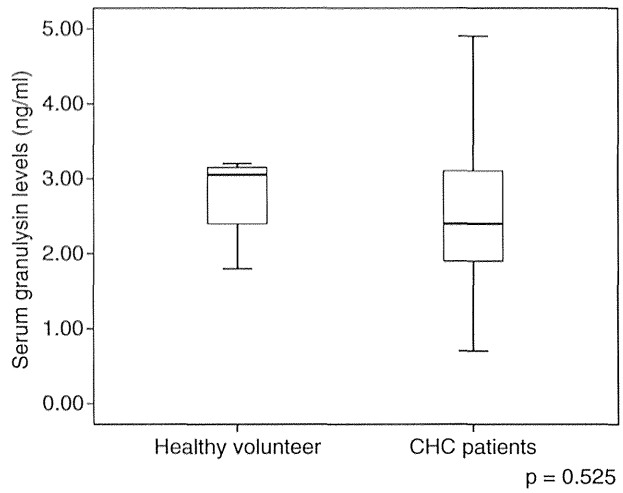

Figure 1 Serum granulysin levels of healthy volunteers and chronic hepatitis C patients. Serum granulysin levels were compared between five healthy volunteers and untreated 20 chronic hepatitis C patients. $P < 0.05$, Mann–Whitney *U*-test.

Univariate analyses identified baseline white blood cell and platelet counts, RVR, and non-grade 3 dermatological reactions significantly associated with SVR (Table 3). Among the nine patients with grade 3 dermatological reactions, three discontinued all treatment and six discontinued telaprevir administration; SVR was achieved in zero of the three (0%) and two of the six (33%), respectively.

Multivariate analysis showed that RVR and non-grade 3 dermatological reactions were significantly associated with SVR (Table 3).

Analysis of risk factors for telaprevir-induced dermatological reactions

Next, we analyzed the association between severe (i.e. grade 3) dermatological reactions and clinical parameters (Table 4). Univariate analysis showed that only sex was significantly associated with the grade 3 dermatological reactions ($P = 0.03$).

Serum granulysin levels in healthy subjects and chronic hepatitis C patients

As shown in Figure 1, serum granulysin levels did not differ significantly between healthy volunteers and chronic hepatitis C patients. Next, we evaluated the association between the severity of dermatological reactions and serum peak granulysin levels in 20 patients including five, four, five and six with grades 1, 2 and 3, and no dermatological events, respectively. One-way ANOVA showed that serum granulysin level was significantly associated with the severity of dermatological reactions ($P = 0.036$); in addition, Tukey's honestly significant difference test revealed that the serum

Table 2 Characteristics of the patients with each dermatological adverse event grade

	n	Age†	Sex (male/female)	Initial telaprevir dose (2250/1500)	Onset of DAR (days)
No DAR	32	61 (28–72)	15/17	26/6	
Grade 1	32	58 (19–73)	15/17	24/8	7 (3–50)
Grade 2	16	61 (44–73)	10/6	12/4	3.5 (1–56)
Grade 3	9	61 (48–65)	8/1	8/1	22 (1–60)

†Data are shown as median range) values.
DAR, dermatological adverse reaction

Table 3 Comparison of the clinical and laboratory characteristics of the patients with HCV infection based on therapeutic response

All patients	SVR	Non-SVR	Univariate analysis	Multivariate analysis		
$n = 89$	$n = 68$	$n = 21$	P	OR	95% CI	P
Age (years)†	60 (19–73)	62 (28–73)	0.402			
Sex (male/female)	37/31	11/10	0.870			
Bodyweight (kg)†	62 (39–97)	64 (32–87)	0.761			
Baseline white blood cells (/μL)†	5135 (1500–9800)	4200 (2490–7200)	0.048	0.492	(0.121–1.993)	0.320
Baseline hemoglobin level (g/dL)†	13.5 (10.5–16.7)	12.1 (9.9–15.4)	0.862			
Baseline platelet count ($\times 10^3$)†	16.7 (6.6–31.5)	12.8 (7.2–86)	0.025	0.388	(0.093–1.614)	0.193
Baseline ALT level (IU/L)†	37 (15–300)	53 (23–159)	0.070			
Baseline HCV RNA level ($\log^{10}$ IU/mL)†	6.7 (3.2–7.6)	6.4 (5.7–7.3)	0.812			
Baseline Cr level (mg/dL)	0.7 (0.5–1.3)	0.7 (0.5–0.9)	0.433			
Initial telaprevir dose (1500/2250 mg)	52/16	17/4	0.460			
Initial PEG IFN dose (1.5/<1.5 μg/kg)	58/10	17/4	0.430			
Initial RBV dose (mg/kg)†	9.9 (2.2–15.5)	9.5 (4.4–12.5)	0.546			
IL28B gene (rs8099917) (TT/non-TT/ND)	43/15/10	8/7/6	0.107			
Core 70 a.a. mutation (wild/mutant/ND)	36/16/16	7/8/6	0.108			
Previous treatment (naive/relapse/NVR)	34/28/6	6/10/5	0.095			
Rapid virological response (+/−)	60/8	10/11	<0.001	10.89	(2.838–41.83)	0.001
Grade 3 DAR (−/+)	66/2	14/7	<0.001	27.44	(3.718–202.5)	0.001

†Data are shown as median (range) values.
a.a., amino acid; ALT, alanine transaminase; CI, confidence interval; Cr, creatinine; DAR, dermatological adverse reaction; HCV, hepatitis C virus; IL28B, interleukin 28B; ND, not done; NVR, non-virological response; OR, odds ratio; PEG IFN, pegylated interferon; SVR, sustained virological response; RBV, ribavirin.

granulysin levels of patients with grade 3 dermatological reactions were significantly higher than those of patients with grade 1 or no dermatological reactions (both $P < 0.05$, Fig. 2).

Time-dependent changes in serum granulysin levels

We investigated the time-dependent changes in serum granulysin levels in five and 15 patients with grade 3 and non-grade 3 dermatological reactions, respectively (Fig. 3). Serum granulysin levels of patients with non-grade 3 dermatological reactions never exceeded 10 ng/ml. Of the five patients with grade 3 reactions, three had severe systemic manifestations that necessitated hospital admission: one each had SJS, DIHS, and systemic lymphoid swelling and high fever (>39 °C). All patients with grade 3 dermatological reactions with systemic manifestations had peak serum granulysin levels exceeding 10 ng/mL; importantly, the serum granulysin levels of two patients already exceeding 8 ng/mL at the onset of the reactions worsened within 6 days.

DISCUSSION

THE PRESENT STUDY demonstrates a significant association between telaprevir-induced dermatological reactions and elevated serum granulysin levels for the first time. Moreover, serum granulysin levels were significantly associated with the severity of dermatological reactions. Thus, the results indicate that serum granulysin level seems to be a useful predictor of telaprevir-induced dermatological reactions. Because the emergence of grade 3 dermatological reactions was significantly associated with non-SVR (Table 3), probably associated with high rate of treatment discontinuation, it is important to predict dermatological events in the early stage to achieve good treatment outcomes.